Nanoscale

PAPER

View Article Online
View Journal | View Issue

Cite this: *Nanoscale*, 2025, **17**, 8690

UV-ozone surface pretreatment for high quality ALD-grown ultrathin coatings on bismuth oxyhalide photocatalysts†

Nitai Arbell, [a,b] Shakked Regev[a,b] and Yaron Paz *[a,b]

The growth of ultrathin layers of oxides by atomic layer deposition (ALD) is well documented for oxide substrates such as SiO_2, Bi_2O_3, Al_2O_3, in which oxygen is the only negatively charged atom. In contrast, the knowledge regarding ALD growth on substrates containing other negatively charged atoms, such as halogens, is quite limited. The commonly used bismuth oxyhalide (BiOX) family of materials are characterised by a low density of surface hydroxyls, required for the initiation of thermal ALD growth of oxides, thus hampering the ability to grow ultrathin layers of oxides on their surface. This restriction becomes even more severe if the process has to be performed at low temperatures. In this work, we show that high quality Al_2O_3 can be grown on bismuth oxyhalide materials by low temperature ALD, upon performing UV-ozone surface pretreatment. The effect of pretreatment on the BiOX photocatalysts was studied by wettability measurements and FTIR. The coating conformality was monitored by both XPS and *via* the ability of the ultrathin layers to suppress the photocatalytic activity of the substrates. The capability to form dense, conformal aluminium oxide layers on BiOX substrates opens a door for low-temperature preparation of organic–inorganic hybrid devices on such and similar compounds.

Received 12th September 2024,
Accepted 6th March 2025

DOI: 10.1039/d4nr03749a

rsc.li/nanoscale

Introduction

In recent years, atomic layer deposition (ALD) has found increasing interest and utilisation in various fields and applications, with the basic aim of growing highly controllable and conformal thin-films on a wide range of substrate types and morphologies. Its high precision in fabricating nanometric thin-films, even on high-aspect ratio surfaces, has given rise to its use in a variety of industries.[1,2] For example, ALD is becoming more and more important in the manufacturing of semiconductor devices, where it is used to grow highly precise, nanometric oxides, such as gate dielectrics in MOSFETs.[3,4] ALD films are also applied in the energy sector, for example as anti-corrosion barriers or protective coatings in batteries.[5,6] These layers are also utilised in the field of catalysis[7,8] and photocatalysis, where they are used as photocatalyst films,[9] protective coatings,[10,11] or activity-lowering dielectric coatings.[12,13] The aforementioned benefits have also made ALD a valuable method in the synthesis of polymer-based hybrid materials,[14,15] as well as in incorporating organic molecules into inorganic structures, as functional moieties[16,17] or as molecular templates.[18,19] These processes require, by their nature, mild conditions and low deposition temperatures, in order to avoid the degradation of the organic components. While low-temperature ALD processes exist for a limited arsenal of compounds,[20,21] generalisation is still a challenge due to difficulties pertaining to the ALD parameters window.

Despite the steadily increasing importance and utilisation of ALD processes in both research and industry, one extremely important aspect is typically not accounted for – the effect of the substrate itself on the resulting films.[22,23] The ideal ALD growth mechanism is based on the Langmuirian adsorption of precursors on the surface of the substrate, and hence highly dependent on the available active groups on the surface, such as surface hydroxyls in the growth of metal oxides.[24–28] Deviations from chemical adsorption result in non-isotropic, non-self-limited growth, leading to non-conformal films.[26,29] There is also a strong effect of the substrate on the deposited layer's properties, such as structure and mechanical strength. This is of particular importance in the ultrathin-layer regime, where interfacial effects are still dominant, and at low deposition temperatures, where chemical bonding to the surface may be hindered. As a result, most mechanistic studies on ALD focus on "simple", well studied substrates, such as Si,

[a]*The Russell Berrie Nanotechnology Institute, Technion-Israel Institute of Technology, Haifa 3200003, Israel. E-mail: Paz@technion.ac.il*
[b]*The Wolfson Department of Chemical Engineering, Technion-Israel Institute of Technology, Haifa 3200003, Israel*

† Electronic supplementary information (ESI) available. See DOI: https://doi.org/10.1039/d4nr03749a

SiO_2, metal oxides or metals.[23,30,31] Some work has been done towards understanding the interplay between ALD and organic polymers, but for them, and for many other families of materials, there are still a lot of uncharted territories.[32,33]

The proven success of ALD in tailoring surfaces is limited by the fact that the number of docking sites in many substrates is too low. In that case, it is important to devise ways for increasing the density of these sites, in order to obtain high quality coatings. In particular, the photocatalytic BiOX family (bismuth oxyhalide, with X representing Cl, Br or I, and occasionally F), presents an interesting challenge, with the use of these materials gaining significant traction in the past decade.[34,35] These materials have excellent photocatalytic activity, part of which relies on a direct charge-transfer mechanism, which differs from "classical" photocatalysts (for example TiO_2), that are based on a surface-hydroxyl mediated mechanism, and have a wide range of halide-dependent bandgap energies, allowing them to be easily tuned for visible-light applications, for example.[36–38] Materials belonging to the BiOX family are easy to synthesise in a variety of morphologies and with well-defined crystal facets.[39,40] Their structure and surface properties are wildly different from traditional ALD substrates, such as oxides and metals, and they do not necessarily display surface hydroxyls, which are typically used as "docking points" for oxide ALD reactions.[25,26] Several methods have been used in an attempt to increase hydroxyl coverage, such as synthesising crystals which primarily expose hydroxylated facets,[41,42] or grafting of organic molecules.[43] These approaches may be suitable for some applications, but might not be appropriate when a conformal ALD coverage of the whole exposed surface is desired. Of specific technological interest is growing an ALD layer around grafted organic molecules adsorbed on the surface of BiOX substrates (or similar materials). In this case the ALD layer can serve as a photoactivity-blocking layer, directing the photoactivity to the non-coated, molecularly imprinted sites, thus enabling highly-selective degradation of target molecules. One such application could be the separation of chiral molecules, which comprise approximately 50% of all active compounds in the pharmaceutical industry.[44]

In this work, we have studied the effect of surface activation on BiOX substrates through UV-ozone cleaning (UVOC) directly before ALD, known to promote hydrophilicity by increasing hydroxyl density,[45–48] similar to the cumulative effect of plasma and humidity in direct bonding.[49] In some ALD processes, ozone is used as the oxidising precursor, shown to induce reactive oxygen species on the surface, allowing for increased reactivity and better coating of these materials.[50] Some previous work has already shown the benefits of UVOC surface pretreatments in the growth of ALD films on MoS_2 and ReS_2 substrates, showing enhanced film conformality by virtue of oxygen atoms grafted onto the surface, resulting in more easily coated surface sites.[51–54] Even more recently, this same technique was applied for the coating of GaN, GeO_2 and SiO_2 substrates, proving to be a simple yet effective method for improving the ALD-grown film properties without inducing significant change to the surface of the substrate itself.[55,56] In almost all cases, the UVOC-coupled ALD process took place at elevated temperatures (200–250 °C) on relatively smooth, non-particulate substrates. To the best of our knowledge, no work has been published regarding the growth of ALD layers on BiOX substrates, let alone on the use of UV-ozone as a mean for improving the quality of such ultra-thin layers.

The effect of different deposition temperatures (within a range that is compatible with growth around grafted organic molecules) was studied, trying to assess the interplay between the ALD window of the precursors and the substrate surface chemistry, which is affected by this temperature as well, through changes in hydroxyl coverage.[57–60] The choice of an optimal temperature is crucial for attaining the best growth conditions for a desired application, as well as for protecting any organic compounds that may be incorporated into the structure for any of the afore-mentioned reasons. To better understand the effect of the UVOC pretreatment in the ultra-thin-layer regime, a number of coatings comprising of different ALD cycle numbers were tested, with thicker layers expected to result in a more conformal layer, as discussed further on in this work.

Due to the high roughness of the substrate, and the extremely low thickness of the deposited layers, typical characterisation techniques such as ellipsometry and AFM are problematic and cannot be reliably used to understand surface properties. Hence, the ALD efficiency and layer conformality were assessed mainly using XPS analysis and kinetic measurements of the photocatalytic degradation of stearic acid. It is believed that these findings can be used for choosing the right combination of substrate and ALD processing conditions, en-route to improving the versatility of ALD-based devices. Of the possible applications of this work, the most interesting for us is the use of BiOX photocatalysts for more precise chemical processes, and especially for the induction of reaction selectivity through molecular imprinting, which benefits significantly from their tuneable bandgaps, allowing working with less energetic light.

Experimental

Preparation of photocatalytic films

Deposition of photocatalytic thin-films. Photocatalytic films were deposited on Si wafers cut into 1″ × 0.5″ (used for investigation of the effect of temperature on the coating) or 0.5″ × 0.5″ (used for investigation of the effect of UVOC treatment) pieces, cleaned with ethanol, acetone and twice with deionised water, followed by immersion in aqua regia for an hour, another deionised water wash, drying overnight at 60 °C, and finally, UVOC treatment (Jelight Company, Inc.) for 10 minutes under humid conditions (a water reservoir inside the cleaning chamber).

BiOX (X = Cl, Br, I) films were grown according to a protocol adapted from Shen *et al.*,[61] with some changes applied. 8 ml of a 2 M aqueous solution of the relevant acid halide (HCl: 32%, Bio-Lab Ltd, HBr: 48%, Fluka Analytical, HI: 55–58%

Thermo Fisher Scientific Inc.) was prepared, with Bi_2NO_3 (99.999%, STREM Chemicals) stirred in to make a 387.5 mg ml^{-1} solution. Ethylene glycol (for analysis, Supelco) and triethanolamine (for analysis, Merck) were added at 2.7 and 4.2% v/v respectively. After stirring overnight, the suspensions were sonicated for 45 min and left to settle. 2 ml of the total volume was removed from the resulting clear supernatant liquid, and 2.66 ml of isopropyl alcohol (AR, Bio-Lab Ltd) were added. A first layer was applied *via* spin coating (Setcas LLC) at 3000 RPM, with overnight drying at 60 °C, followed by deposition of a second layer, resulting in an optically-thick coating. TiO_2 films were also grown as a reference, according to a published sol–gel process.[62] Here, two subsequent layers were deposited by spin-coating at 1500 RPM, with intermittent calcination.

In an attempt to gain a better understanding of the distribution of ALD-grown alumina on top of different materials, a second set of samples was prepared. The films in this set were composed of BiOX particles, synthesised solvothermally according to a previously established protocol,[63] dispersed in a silica binder, were tested. The surface area of the powders was measured using BET isotherms (FlowSorb II2300, Micrometrics Ltd) as 1.5, 5.6 and 50.3 m^2 g^{-1} for the synthesised BiOCl, BiOBr, BiOI respectively. The silica binder was made by the sequential, dropwise addition of 1.085 ml LUDOX (30%, Merck), 17 μl of HCl (32%, Bio-Lab Ltd), and 3.19 ml isopropyl alcohol (AR, Bio-Lab Ltd) into 0.71 ml tetraethyl orthosilicate (TEOS, 98%, Sigma Aldrich). Aqueous suspensions of the BiOX particles were made by separately mixing either 196.1 mg BiOCl, 228.7 mg BiOBr or 263.25 mg BiOI each in 250 μl deionised water, followed by 15 minutes of ultrasonication. 138 μl silica binder and 328 μl 1-propanol (analysis grade, Supelco) were then added to each suspension, followed by another 30 minutes of ultrasonication. 100 μl of each suspension was then spun for 1 minute at 4000 RPM in two consecutive layers on top of cut and cleaned glass slides, resulting in an optically thick film.

UV-ozone pretreatment and ALD coating. A portion of the prepared films were UVOC-treated for 10 minutes, typically with a water reservoir in the chamber to increase surface hydrophilation ("wet UVOC"), except for samples used to investigate the effect of water presence during UVOC, which were treated without any added water in the chamber ("dry UVOC"). Additional films were further processed as they were, without any UVOC pretreatment. All the films apart from the controls were then overcoated with Al_2O_3 by thermal ALD using a custom-built system, designed with VST Services Ltd, with trimethylaluminium (TMA) and H_2O as precursor and oxidiser respectively, and argon as the carrier gas. The full procedure was as follows: introducing the films into the reaction chamber, pumping down to base pressure (0.01 torr) and heating of the sample stage to the desired temperature (40, 60, 80 °C) for 45 minutes, to achieve thermal equilibrium. Next, 1, 5, 10, or 20 cycles of alternately pulsed TMA and H_2O were applied. The pulse lengths were 0.1 second, separated by 10 seconds of argon purging.

Characterisation

FTIR measurement. FTIR measurements were performed under vacuum using a Vertex 70v FTIR (Bruker Ltd), equipped with a DTGS detector and a 6 mm aperture. Here, 200 mg of KBr were dried for 1 hour at 60 °C before grinding with a mortar and pestle, and placed in a hydraulic press for 1 hour under a load of 5 tonnes at RT. 5 mg of solvothermally prepared BiOX particles were ground and deposited on the prepared KBr pellets before being placed once again in a hydraulic press for 30 minutes under a load of 5 tonnes at RT, to achieve a thin and uniform coverage of the pellet surface. BiOX films were compared to a KBr background, with each sample measured twice, once after desiccation, and once immediately after, following UVOC-treatment for 10 minutes with a water reservoir in the chamber. An additional control was measured, of a KBr pellet before and after the same UVOC treatment, compared to a vacuum background.

Contact angle measurement. Wettability measurements were performed with water by an OCA 15Pro system (DataPhysics Instruments GMBH). For these measurements, 200 mg of each powder of solvothermally prepared BiOX particles was ground in a mortar and pestle, placed in a hydraulic press for 1 hour under a load of 7.5 tonnes while heated to 150 °C, and fully cooled and desiccated before measurement. The result was a smooth and stable BiOX pellet. For each type of BiOX, one pellet was measured as prepared (following cooling and desiccation), while the other was measured immediately after being UVOC-treated for 10 minutes with a water reservoir in the chamber. Deionised water drops of a volume of 120 μl and above were deposited at a rate of 3 μl sec^{-1}, with the measured contact angle averaged over more than 200 readings per sample.

Scanning electron microscopy (SEM) and energy dispersive X-ray spectroscopy (EDS). EDS and SEM analyses were performed using a Helios NanoLab DualBeam G3 UC system (FEI Company) operating at 25 kV.

X-ray photoelectron spectroscopy (XPS). XPS measurements (in both survey mode and HR mode) were performed using a Versaprobe III system (Physical Electronics Inc.), using a focused X-ray AlKα monochromated X-rays source, operating at a 200-micrometre beam size, 50 W, and 15 kV. Dual beam neutralisation was employed to negate surface charging effects and avoid the use of a charge reference. The lack of charging effects was verified using the C 1s peak at 248.8 eV. Each sample was measured at two points, except for the BiOI samples (with and without UVOC pretreatment) coated with 10 ALD cycles, which were measured at one point due to operator constraints.

Photocatalytic degradation testing. The photocatalytic kinetics were investigated according to a previously described method using the apparent zero order degradation of stearic acid, monitored under vacuum using a Vertex 70v FTIR (Bruker Ltd), equipped with a DTGS detector and a 6 mm aperture.[62,64,65] Samples of ALD-coated BiOX films on Si wafers were placed in parallel under a wide-band, 365 nm-

centred UV fluorescent lamp, at a flux of 0.4 mW cm^{-2}. Each measured film was compared to non-ALD coated controls, fabricated as part of the same synthesis batch. For most cases, three replicates were used.

Results and discussion

SEM and EDS characterisation

Fig. 1A1 presents SEM micrographs taken from a substrate made of a film of BiOCl particles in a silica binder, coated with alumina by 10 ALD cycles grown at 80 °C, using trimethylaluminum as reactant 1 and water as reactant 2 (oxidiser). Here, Fig. 1A1 shows a sample in which the ALD process was performed without a UVOC pretreatment, whereas Fig. 1A2 depicts a sample that was subjected to wet-atmosphere UVOC pretreatment prior to growing the first ALD layer. Fig. 1B–E display the EDS maps of O, Al, Bi, Cl, respectively, corresponding to the samples prepared without and with UVOC pretreatment. The images were taken deliberately in the absence of a conductive coating, despite the effect of charging on the image quality. As shown in the insets of Fig. 1, the various types of atoms are more or less evenly distributed in the samples. No significant difference was observed between samples that were subjected to pretreatment and samples that were prepared without pretreatment. This observation was general for all types of BiOX substrates, regardless of ALD-growth temperature (see ESI S1–S10†). Likewise, micrographs taken from films prepared on substrates comprising of only BiOX, coated with alumina by ALD, showed an even distribution of Al (ESI S11–S13†). While these results seem to point towards no discernible effect of the UVOC pretreatment, this was not the case when using methods that are more sensitive to atomic concentration differences or to coating conformality at the nanoscale, as will be shown in the following results.

Contact angle measurement

The effect of UVOC treatment on surface properties was carried out using optical contact angle measurements of water on pure, smooth-surfaced BiOX pellets. Fig. 2A–C present images of water droplets on BiOCl (A), BiOBr (B) and BiOI (C), prior to (indexed as 1) and immediately after UVOC treatment (indexed 2). The photographs clearly show the decrease in the water contact angles on the various BiOX surfaces upon exposure to the UV-ozone treatment. The increased hydrophilicity of the surfaces is depicted in Fig. 2D, presenting the averaged measured contact angles. Here, contact angle measurements gave values of 55 ± 1°, 53 ± 1° and 63 ± 1° for BiOCl, BiOBr and BiOI, respectively, prior to UVOC exposure, and 25 ± 3°, 31 ± 3° and 21 ± 1°, respectively, following UVOC treatment. As can be seen, the effect was most significant for the BiOI samples, which showed both the largest drop in contact angle, and the lowest absolute contact angle following UVOC treatment, and least significant for the BiOBr samples.

FTIR analysis

In order to further understand the effects of UVOC treatment on the surface properties of bismuth oxyhalides, thin layers of BiOX were pressed onto KBr pellets, enabling a smooth surface, adequate for FTIR measurements. The pellets were measured prior to and immediately after UVOC treatment (Fig. S14 and S15†). The difference spectra, obtained by subtracting the pre-UVOC treatment spectra from the post-UVOC treatment spectra, are presented in Fig. 3 for BiOCl (A), BiOBr (B) and BiOI (C). In all cases, the difference spectra reveal negative peaks in the 700–1500 cm^{-1} range. This region is attributed to transitions in the Bi–X vibrational modes,[66–68]

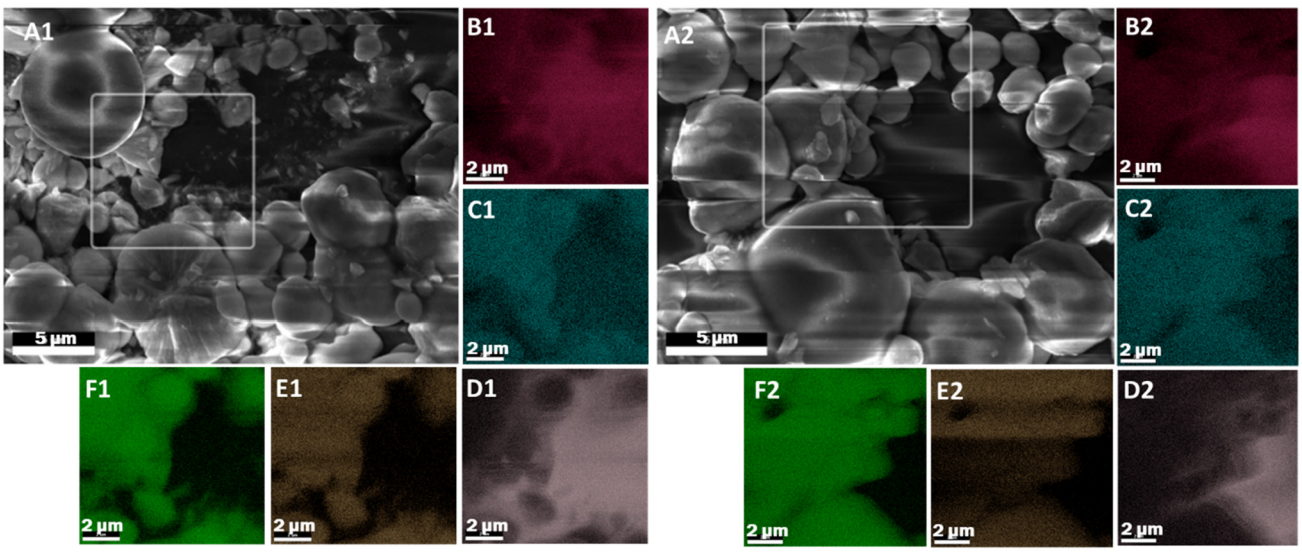

Fig. 1 (A) SEM micrograph and (B–F) EDS elemental maps of the highlighted area for BiOCl in an SiO_2 binder coated with 10 cycles of Al_2O_3 ALD at 80 °C without (A1–F1) and with (A2–F2) UVOC pretreatment. EDS legend: O (B), Al (C), Si (D), Bi (E) and Cl (F) atoms.

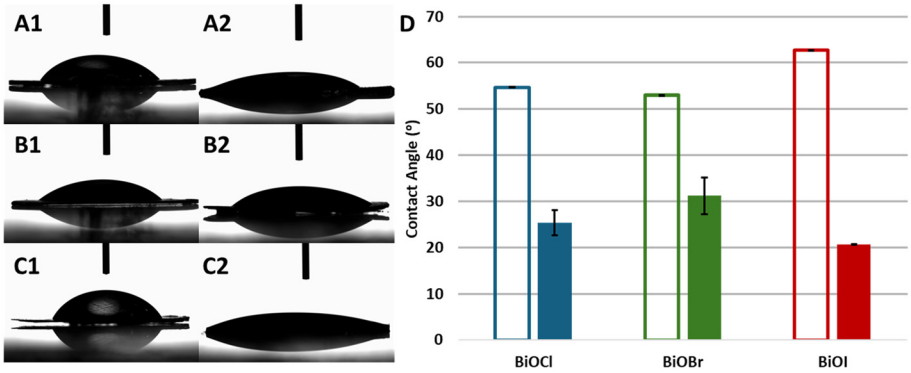

Fig. 2 (A–C) Images of the water droplets deposited on BiOCl (A), BiOBr (B) and BiOI (C) pellets, prior to (1) and immediately following (2) UVOC treatment. (D) Averaged water contact angles measured on pure, non-coated BiOX pellets, prior to (empty bars) and immediately following (filled bars) UVOC treatment.

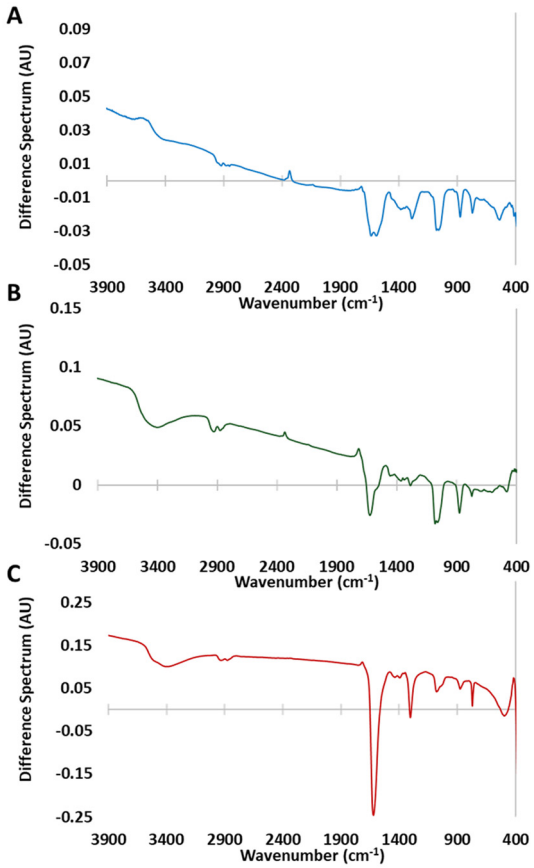

Fig. 3 Difference spectra of thin BiOX films pressed on KBr pellets, obtained by subtracting of the FTIR spectra measured before UVOC treatment from the spectra recorded following UVOC treatment, for BiOCl (A), BiOBr (B), and BiOI (C).

hence the spectral changes can be interpreted as indicating some loss of Bi–X bonds. Another negative peak is observed at 1620 cm^{-1}. This peak is attributed to an H–O–H bending mode, suggesting a decrease in the amount of adsorbed water. This decrease is somehow surprising as the opposite would be expected, based on the observed increase in hydrophilicity (Fig. 2). One possible explanation for the overall spectral changes could be the substitution of surface halogens with hydroxyl groups, while emitting HX species.

XPS analysis

The averaged atomic percentages of the various elements, was deduced from XPS measurements in survey mode performed on films coated with 1, 5 and 10 ALD cycles of alumina at 60 °C with and without UVOC pretreatment. These values are shown in Fig. 4. As seen in the Figure, for 10 ALD cycles, and in all BiOX types, the atomic concentration of aluminium in films prepared with a UVOC pretreatment step was very similar (if slightly higher) to that of films prepared without this step, and ranged between 11.3% to 14.4%, with the Al prevalence ratio between pretreated and non-pretreated samples taking on values of 1.18 for BiOCl, 1.05 for BiOBr, and 1 for BiOI. The ratio between bismuth and halogen atoms was in all cases higher than expected (1.16 in BiOBr to 1.74 in BiOI). This may be explained by the replacement of some halogens during the formation of the alumina layer, and possibly also during UVOC pretreatment as inferred also from our FTIR results (Fig. 3). Alternatively, it could be due to some systematic error in the XPS sensitivity factor. The atomic concentration of oxygen (62.6% to 70.7%) was higher than expected from combining the stoichiometry of alumina and BiOX (approximately 32%), perhaps due to water adsorbed on the alumina surface.

To try and probe the effect in thinner layers, where the signal from the BiOX-alumina interface is more apparent, the same analysis was performed on BiOX films coated with 5 ALD cycles of alumina. As can be seen in the Figure, the aluminium content was again found to be quite similar for samples that have undergone UVOC pretreatment and those that have not undergone this step, yet with a somewhat larger prevalence of aluminium in all samples that underwent surface treatment relative to those that have not, with the Al prevalence ratio between pretreated and non-pretreated samples taking on values of 1.01 for BiOCl, 1.08 for BiOBr, and 1.11 for BiOI. The aluminium percentages deduced for these samples was larger

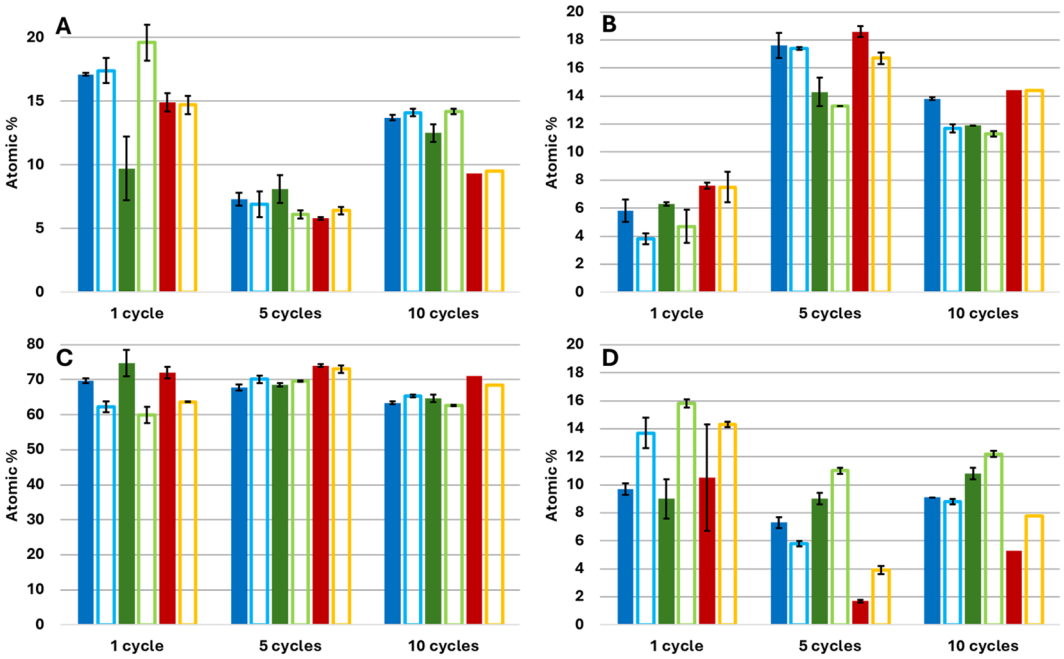

Fig. 4 XPS atomic percentage of bismuth (A), aluminium (B), oxygen (C), and the relevant halide (Cl, Br or I) (D) as measured by XPS (in survey mode) for 1, 5 and 10 cycle ALD coatings grown at 60 °C with (full bars) and without (empty bars) UVOC pretreatment, shown on a carbon-free basis. Shades of blue denote BiOCl samples, shades of green denote BiOBr samples, and red/orange denote BiOI samples.

than that of the 10 cycle ALD films, ranging between 13.3% to 17.6%, at the expense of lower prevalence for bismuth and halide atoms. The bismuth to halogen ratio varied significantly in these samples (roughly 0.55 in BiOBr, 1 in BiOCl, to 3.4 in BiOI); again, the reason is unclear to us. Oxygen prevalence remained in a similar range (67.8% to 74.0%), still higher than expected based on the stoichiometry of the combined films (approximately 34%). Again, adsorbed water could be the reason for this larger oxygen prevalence.

Upon working with even thinner layers of 1 ALD cycle, a stronger effect of the UVOC pretreatment can be seen. Here, pretreated samples showing a larger prevalence of aluminium atoms relative to those that have not undergone this step, with values lower than those for 5 and 10 ALD cycles, in the range of 3.8% to 7.6%, and Al prevalence ratios between pretreated and non-pretreated samples of 1.53 for BiOCl, 1.34 for BiOBr, and 1.01 for BiOI. Additionally, it can be seen in all BiOX samples that there is a major increase in the prevalence of oxygen atoms in samples exposed to the pretreatment step. The atomic concentrations of oxygen, averaged over all BiOX types, were 62.0 ± 1.5% and 72.2 ± 2.1% for non-pretreated and pretreated samples, respectively. The bismuth to halogen ratio was higher than expected in all cases (roughly 1.7 for BiOCl, 1.2 for BiOBr, and 1.4 for BiOI). The averaged Bi/X ratio was 1.42 for the pretreated samples, whereas for the non-treated this ratio was considerably lower (1.20), supporting the notion that a possible consequence of the UVOC treatment was partial substitution of halogens with hydroxyls originated from water.

High-resolution XPS analysis of the peaks (Fig. 5, 6 and Fig. S16–S19†) shows in more detail the chemical differences between samples coated with and without UVOC pretreatment. As shown in Fig. 5, for samples coated with 1 ALD cycle at 60 °C, significant chemical shifts were noted between the samples, most notably so for O and X (Cl, Br or I) atoms (for clarity, the deconvolutions of the peaks are given in the ESI, Fig. S20–S25†). For the O 1s peak in BiOCl and BiOBr (Fig. 5A3 and B3), an increase in the ratio between the higher binding energy peak (around 532 eV), corresponding to hydroxyl-terminated aluminium,[69] and the lower binding energy peak (around 530 eV), corresponding to stoichiometric Al_2O_3, can be noted for samples which underwent UVOC pretreatment. For BiOI however, the apparent effect is the opposite, with a relative increase in the Al_2O_3 oxygen peak relative to the hydroxyl one. This suggests a different mechanism governing the ALD growth of alumina on the surfaces of the catalysts. Perhaps the strongest evidence for the chemical effect of the UVOC pretreatment can be found in the halogen curves, where pretreated BiOCl and BiOBr both show a relative increase in the higher binding energy peaks corresponding to lower-spin states ($2p_{1/2}$ for Cl and $3d_{5/2}$ for Br), while in BiOI, a completely new peak emerges at 622.3 eV in the pretreated sample, corresponding to high-oxidation state (+5 or +7) iodine. This points to a possible role of the iodine in the chemical changes occurring on the BiOI surface following UVOC pretreatment. Some minor changes can also be noted in the Al spectra, where BiOCl and BiOBr show a slight shift of the peak to higher binding energies following UVOC pretreatment, while BiOI

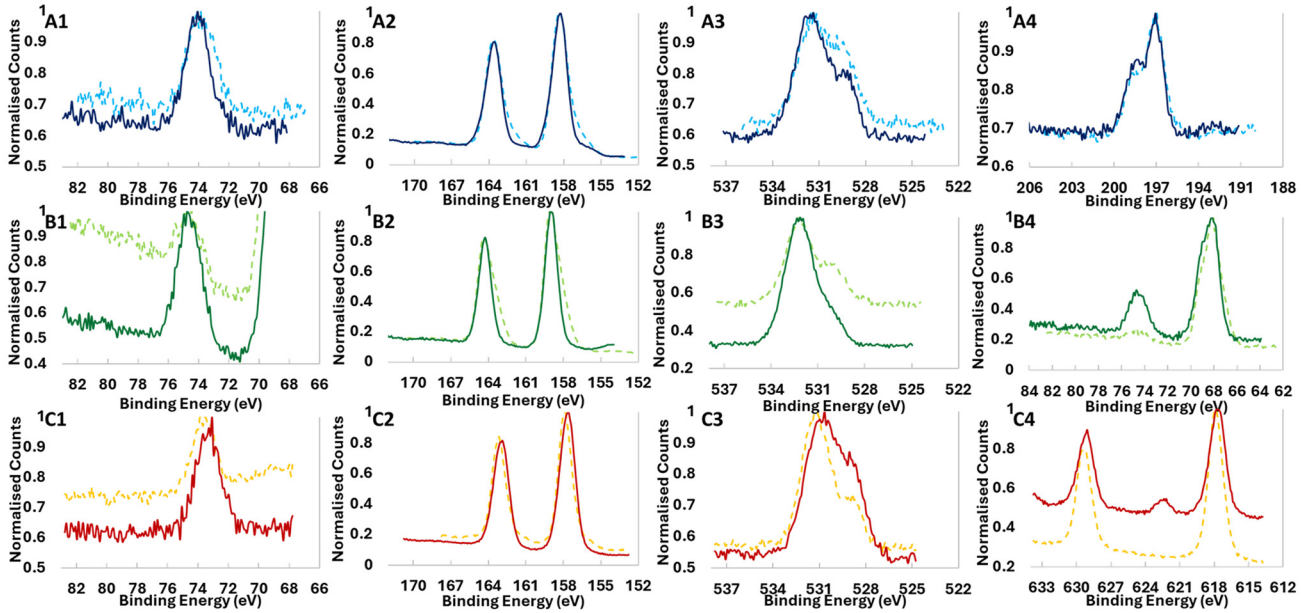

Fig. 5 High resolution XPS curves of: (A) BiOCl, (B) BiOBr and (C) BiOI coated with 1 cycle of ALD at 60 °C. Traces corresponding to Al, Bi, O and X (Cl, Br or I) atoms are denoted by indexes of 1–4, respectively. Continuous curves represent samples coated following UVOC pretreatment, while dashed curves represent samples coated without UVOC pretreatment.

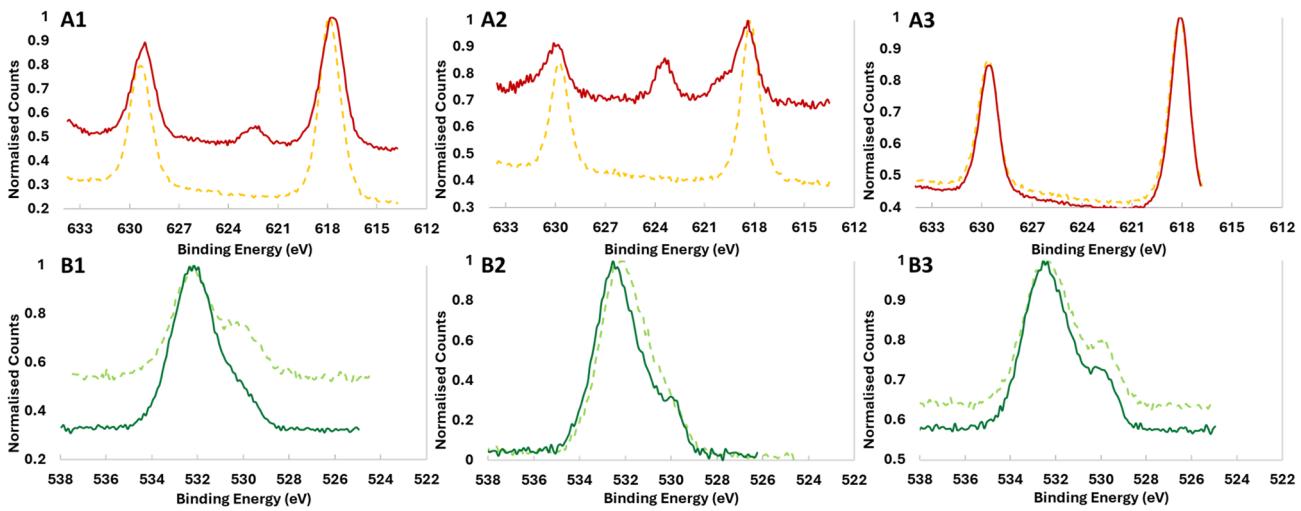

Fig. 6 High resolution XPS curves of: (A) I atoms in BiOI, (B) O atoms in BiOBr. Coating by 1 cycle, 5 cycles, or 10 cycles of ALD at 60 °C is denoted by indexes of 1–3, respectively. Continuous curves represent samples coated following UVOC pretreatment, while dashed curves represent samples coated without UVOC pretreatment.

again shows the opposite effect, with the peak shifting to lower binding energies. The peaks in the Bi spectra remain pretty much unchanged for BiOCl and BiOBr, while BiOI displays a shift to lower binding energies following UVOC pretreatment.

HR-XPS results for samples with different ALD cycle numbers show the enhanced importance of this effect at the ultrathin-film regime, *i.e.*, at low cycle numbers. As exemplified in Fig. 6, at 1 ALD cycle the I spectra in BiOI (Fig. 5A1) and O spectra for BiOBr (Fig. 5B1) are quite different for pre-treated and non-pretreated samples, with differences remaining present in 5 ALD cycles, but vanishing at 10 ALD cycles.

Photocatalytic degradation testing

In principle, an indication on the quality of the ALD layers may be obtained *via* direct imaging by TEM. However, attempts at applying this method failed due to the relatively weak adhesion of the BiOX particles, which prevented excavating sufficiently thin lamellae by Focused Ion Beam (FIB). Likewise, AFM and Ellipsometry were found to be ineffective,

due to the relatively large roughness of the films, which did not allow obtaining reliable results, considering the low thickness of the ALD films. In the absence of appropriate characterisation alternatives, we have used photocatalysis as a probe for the conformality of the adlayer, to further demonstrate the effect of a UVOC pretreatment on the quality of ALD-grown layers. Here, coating a photocatalyst with an inert layer is expected to mitigate its photoactivity, depending on adlayer thickness and conformality. Fig. 7A presents changes in the IR spectrum of a stearic acid (SA) film deposited on an alumina-coated BiOBr substrate, following exposure to UV light. As shown in the figure, the photocatalytic degradation is manifested by a decrease in the intensity of the CH_2 ν_a and ν_s peaks. Accordingly, by plotting the intensity of the CH_2(s) peak as a function of irradiation time, it is possible to deduce the kinetics of degradation, found to be of an apparent zero order rate law (Fig. 6B). Such a rate law is quite common for the photocatalytic degradation of a multilayer of stearic acid.[62,64,65] These slopes were used to assess the quality of the alumina coatings.

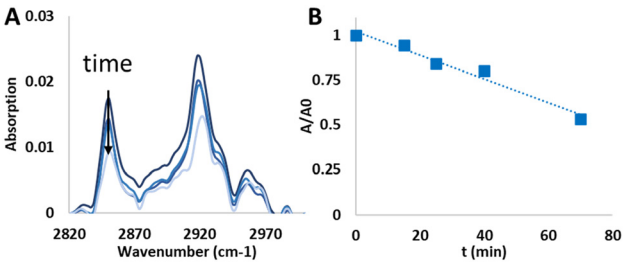

Fig. 7 (A) FTIR spectra of stearic acid degradation over a BiOCl substrate that was coated with 10 cycles of Al_2O_3 ALD, following UVOC pretreatment, (B) the absorption of the stearic acid (A), normalised by its initial absorption (A_0) as a function of UV-exposure time. As portrayed in the figure, these kinetics are fitted to a zero-order rate law.

Any study of the effect of ALD growth parameters of alumina on the activity damping of the underlying photocatalyst should take into account the fact that the photocatalytic activity of the substrates varies among the different types of photocatalysts. Fig. 8A presents the measured zero-order rate constant for the various BiOX photocatalysts, as well as that of TiO_2, used as a benchmark which contains a high density of hydroxyls on its surface. These values were used to normalise the rate constants of the ALD-coated samples. Depicted in Fig. 8B–F are the normalised rate constants for catalysts coated with 10 ALD cycles. It should be noted again that all measurements were performed on optically-thick photocatalytic films, such that all impinging photons are absorbed. This negates the possibility for inaccuracies due to small deviations in the thickness of the photocatalytic underlayer. For each photocatalyst, activity was measured both for samples prepared with a UVOC pretreatment and for samples prepared without pretreatment. Here, three ALD temperatures were examined: 40 °C, 60 °C and 80 °C, all of which can be considered as low process temperatures, adequate for the growth of organic–inorganic hybrid devices. As expected, in all cases, the normalised rate was lower than one, demonstrating activity damping by the alumina overlayer. A comparison of the average damping, over all conditions, between the various

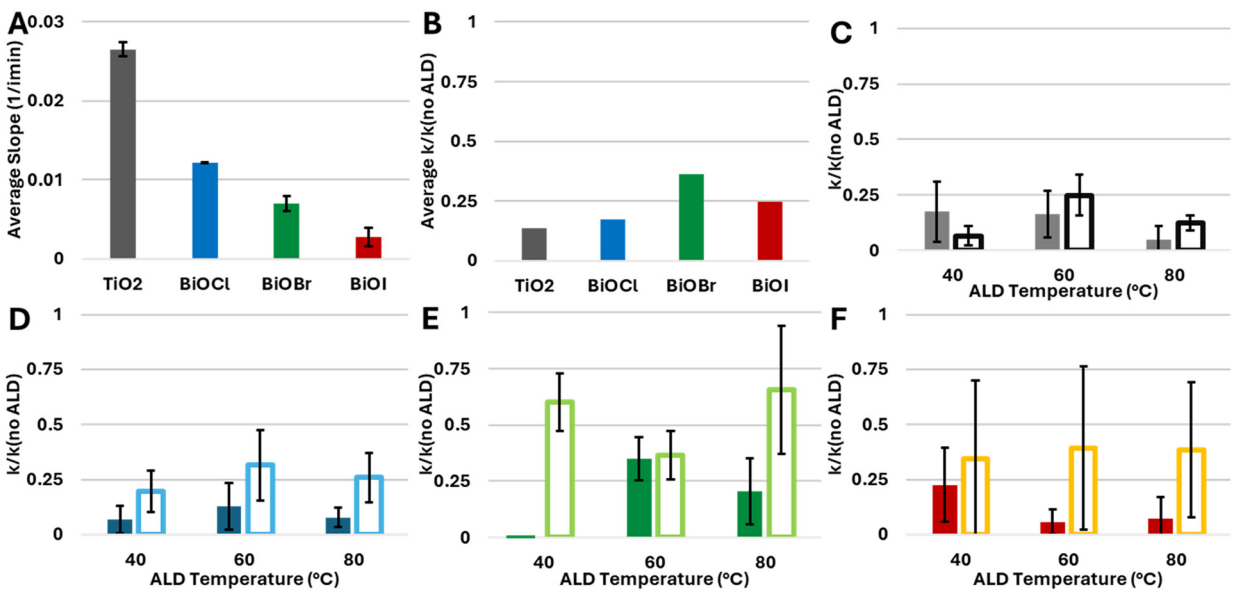

Fig. 8 (A) The average slopes for the photodegradation of stearic acid (*i.e.*, normalised zero order rate constants), measured for uncoated photocatalysts. (B) The ratio between the normalised zero-order rate constants of samples coated with 10 ALD cycles, averaged over all coating parameters, and the rate constants for the corresponding uncoated samples. (C–F) The ratio between the normalised zero-order rate constants of samples coated with 10 ALD cycles, and the rate constants for the corresponding uncoated samples. Data is given for TiO_2 (C), BiOCl (D), BiOBr (E) and BiOI (F), coated at three deposition temperatures (40 °C, 60 °C, and 80 °C). Filled bars in figures C–F represent samples that underwent UVOC pretreatment, while empty bars represent samples that did not undergo pretreatment.

types of photocatalysts (Fig. 8B), reveals that the activity damping in titania was considerably more pronounced than that of the three types of BiOX photocatalysts. This difference can be explained by a more compact alumina layer, relatively free of pinhole defects, formed by virtue of the high density of hydroxyls on the TiO_2 surface during the growth of the first layer.

The results portrayed in Fig. 8C–F clearly show that performing the UVOC pretreatment led to higher damping of the photocatalytic activity, thus indicating an improvement in the conformality of the ALD film. While this observation is correct for all BiOX photocatalysts, under all three temperatures of Al_2O_3 deposition, TiO_2 seems to behave differently when coated at 40 °C at which damping was higher for the non-pretreated substrates. Analysing the data obtained from samples whose inert layers were grown at different temperatures does not reveal any concrete dependence of the activity damping on the deposition temperature. This may indicate, alas not prove, the presence of hidden parameters having contradictory influence.

For 10 ALD cycles, averaging over all preparation temperatures and BiOX types, the introduction of a UVOC pretreatment step decreased the activity by a factor of three. For TiO_2, this effect was somewhat muted, reflecting the notion that (at least at low temperatures) there was no need for increasing the density of surface hydroxyls.

To better understand the interaction between coating thickness and surface pretreatment in the activity damping of the substrate, similar measurements were performed on samples coated with 5 and 20 ALD cycles, all performed at 60 °C, as shown in Fig. 9. The figure clearly shows that the reduction in activity induced by the UVOC pretreatment was not limited to alumina films formed by 10 ALD cycles, but it is rather general, as it can be observed also with thinner films (prepared by five ALD cycles), as well as with thicker films (prepared by twenty ALD cycles). As can be seen in the figure, and as was expected, increasing the coating thickness resulted in increased activity damping, in all cases (except for BiOBr coated with 10 ALD cycles). Generally speaking, the photocatalytic activity of pretreated substrates, overcoated by five ALD cycles, was reduced by roughly 75%, whereas twenty ALD cycles was sufficient to reduce the activity to practically zero.

As a final point of comparison, it was decided to test the influence of performing the UVOC pretreatment in the absence of a humid atmosphere, *i.e.*, without the addition of a water vessel to the chamber. This was carried out for substrates coated by five ALD cycles and twenty ALD cycles. The comparison between samples undergoing wet and dry pretreatment prior to ALD coating at 60 °C is shown in Fig. 10. As can be seen from Fig. 10A–C, there was no observable effect of the inclusion of a water vessel in the cleaning chamber, and the samples showed the same activity damping for both "dry" and "wet" pretreatment. This points to ambient moisture and the generated ozone being sufficient in order to activate the surface, without necessitating the addition of more water to the system. The deviation of BiOI from this trend is apparently in line with the HR-XPS results shown above, which pointed towards surface hydroxyls being less important for the coating conformality on this material, with enhanced hydroxylation possibly even harming ALD performance.

Finally, to ensure the statistical significance of our finding that UVOC pretreatment improves the conformality of ALD-grown alumina overcoating BiOX substrates, T-tests were performed on the results obtained for BiOX catalysts coated at 60 °C for all three coating thicknesses used in this work (Table S1†). The *p*-values, averaged over all three types of BiOX photocatalysts, were found to be 0.0151, 0.0488 and 0.0639 for alumina layers grown by 5, 10 and 20 cycles, respectively. The results clearly support our claims. It should be noted that the thinner the layers are, the lower is the *p*-value. This indicates that the beneficial effect of the UVOC pretreatment is more pronounced for thin layers and becomes less measurable as the coating becomes thicker.

The proposed effect of the UVOC pretreatment on the growth of alumina by ALD, as suggested based on the XPS and photocatalytic kinetic results, is illustrated in Fig. 11. In the

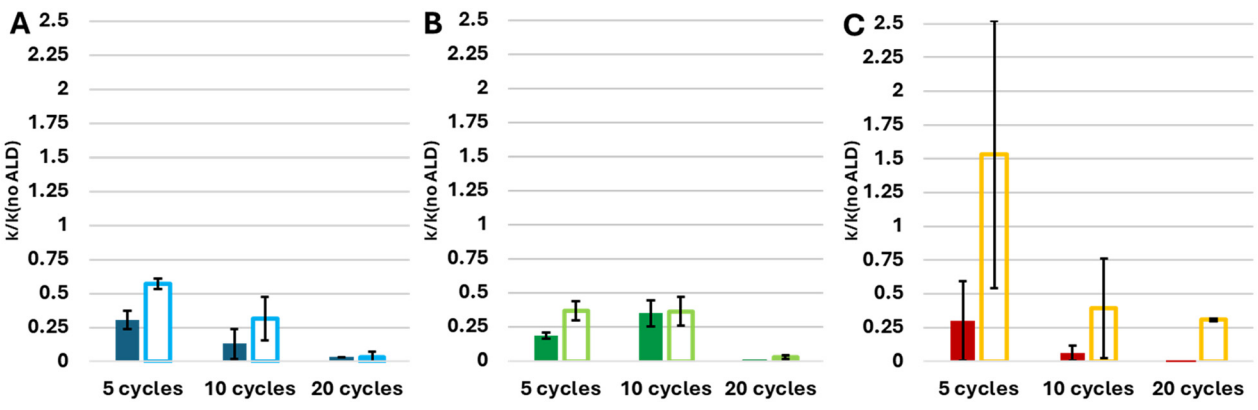

Fig. 9 The ratio between the normalised zero-order rate constants of samples coated with alumina by ALD at 60 °C to the rate constants for the corresponding uncoated samples. Data is given for (A) BiOCl, (B) BiOBr and (C) BiOI, coated with either 5, 10 or 20 ALD cycles. Filled bars represent samples that underwent UVOC pretreatment, and empty bars represent samples that did not undergo pretreatment.

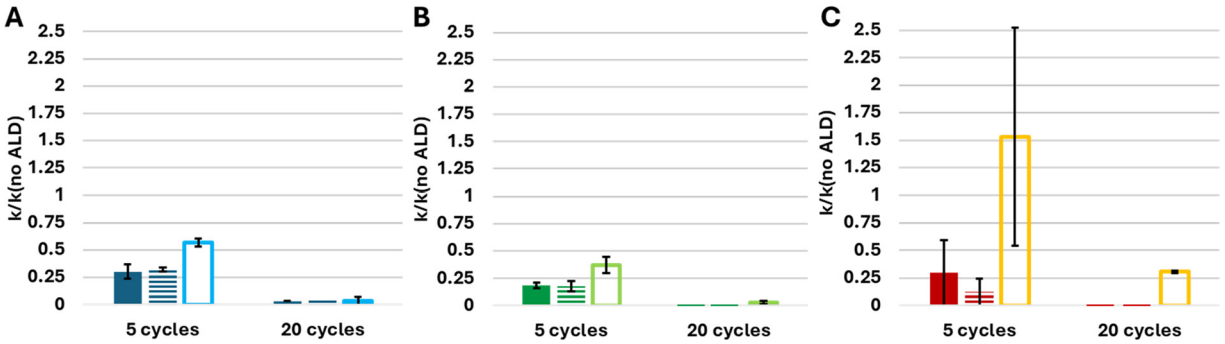

Fig. 10 The ratio between the normalised zero-order rate constants of samples coated with alumina by ALD at 60 °C to the rate constants for the corresponding uncoated samples. Data is given for (A) BiOCl, (B) BiOBr and (C) BiOI, coated with either 5 or 20 ALD cycles. Filled bars represent samples that underwent wet UVOC pretreatment, striped bars represent samples that underwent dry UVOC pretreatment, and empty bars represent samples that did not undergo pretreatment.

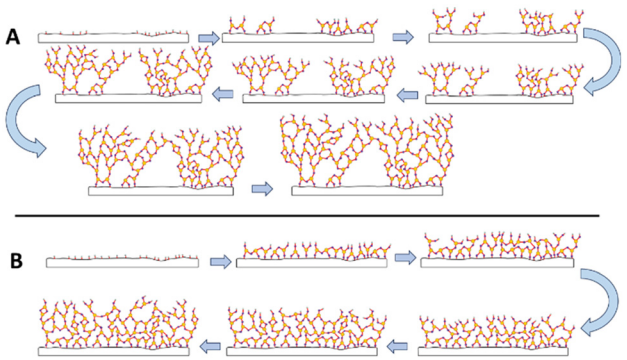

Fig. 11 Illustration of the proposed layer-by-layer growth of alumina on BiOX substrates in the absence of (A) and following UVOC pretreatment (B). For clarity, and due to the reduced dimensionality of the illustration, the coordination numbers of aluminium and oxygen were set to 3 and 2, respectively, instead of 6 and 4.

absence of pretreatment (Fig. 11A), the anchoring of the aluminium atoms in the first layer is inadequate, leading to incomplete coverage. Successive layers partially bridge-over these voids, reaching aluminium density that approaches that of a well-packed layer, as appeared in XPS measurements, within approximately 10 ALD cycles. Still, the underlying pores, and the less rigid structure, enable mass transport through the layer, manifested by reduced blocking of photocatalytic degradation. The introduction of UV-ozone cleaning of the surface increases the density of anchoring points on the surface, makes the first layer to be highly conformal and well-packed. Consequently, mass transport through the layer is hampered, leading to dampened degradation kinetics of the stearic acid (Fig. 11B).

Conclusions

This research shows, for the first time to our knowledge, the ALD growth of aluminium oxide on bismuth oxyhalides and, in particular, at low temperatures (40–80 °C). The deposition performed here was in the ultrathin regime (1–20 ALD cycles), where substrate effects are most apparent. It is reported hereby that UV-ozone pretreatment of the BiOX surfaces prior to ALD coating improves the quality of the coating significantly. While SEM-EDS was found to be silent with respect to the quality and conformality of such layers, wettability measurements and FTIR indicated that the UV-ozone treatment increases the hydrophilicity of the BiOX surface, most likely by replacing part of the halogens with hydroxyl groups. XPS survey revealed differences between ALD layers deposited following pretreatment and ALD layers grown without pretreatment. These differences were manifested by higher atomic percentages of Al and O in the pretreated samples. HR-XPS further revealed chemical differences between substrates that have undergone UVOC pretreatment to those that have not. These differences were most evident with ultrathin layers made of a single ALD cycle, and gradually disappear upon increasing thickness. Using photocatalysis as a tool for investigation of mass transport through the overcoating inert layer revealed that exposing the surface of the substrate to UV-ozone environment had a significant beneficial effect on the quality of the grown layers, especially at very low thicknesses. These results point to an initial growth of non-conformal layers for non-pretreated samples, that are bridged over at higher cycle numbers, as opposed to a growth mode of higher quality films from the outset for samples whose surface was activated by UVOC pretreatment. This finding paves the way for the development of oxide ALD layers on oxide substrates that contain non-oxygen negatively charged atoms, such as halogens. Moreover, the capability to form dense, conformal aluminium oxide layers on these substrates at low temperature opens a door for the preparation of hybrid organic–inorganic devices on BiOX compounds. Such devices are currently under study, and will be reported elsewhere.

Author contributions

N. Arbell conceived and carried out all aspects of this research, including characterisation, synthesis, analysis and

writing. S. Regev performed part of the measurements. Y. Paz supervised NA and SR and participated in the analysis of the data and in writing the manuscript.

Data availability

The data supporting this article have been included as part of the ESI.†

Conflicts of interest

There are no conflicts to declare.

Acknowledgements

The authors would like to thank Dr Kamira Weinfeld, Ms Lital Felzenshtein and Mr Gideon Onuh for their help with the technical aspects of this project. Additional thanks are given to the Russell-Berrie Nanotechnology Institute for using their facilities and for their financial support.

References

1 S. M. George, *Chem. Rev.*, 2010, **110**, 111–131.
2 V. Cremers, R. L. Puurunen and J. Dendooven, *Appl. Phys. Rev.*, 2019, **6**, 021302.
3 K. Y. Chen, C. C. Yang, C. Y. Huang and Y. K. Su, *RSC Adv.*, 2020, **10**, 9902–9906.
4 H. Y. Shih, F. C. Chu, A. Das, C. Y. Lee, M. J. Chen and R. M. Lin, *Nanoscale Res. Lett.*, 2016, **13**, 235.
5 J. Liu and X. Sun, *Nanotechnology*, 2014, **26**, 024001.
6 Y. Cao, X. Meng and A. Li, *Energy Environ. Mater.*, 2021, **4**, 363–391.
7 X. Wang, Z. Zhao, C. Zhang, Q. Li and X. Liang, *Catalysts*, 2020, **10**, 1298.
8 B. J. Oneill, D. H. K. Jackson, J. Lee, C. Canlas, P. C. Stair, C. L. Marshall, J. W. Elam, T. F. Kuech, J. A. Dumesic and G. W. Huber, *ACS Catal.*, 2015, **5**, 1804–1825.
9 N. K. R. Eswar, S. A. Singh and J. Heo, *J. Mater. Chem. A*, 2019, **7**, 17703–17734.
10 H. Krýsová, M. Neumann-Spallart, H. Tarábková, P. Janda, L. Kavan and J. Krýsa, *Beilstein J. Nanotechnol.*, 2021, **12**, 24–34.
11 D. Liu, Y. Liu, S. L. Candelaria, G. Cao, J. Liu and Y. H. Jeong, *J. Vac. Sci. Technol., A*, 2012, **30**, 01A123.
12 K. Pham, S. Pelisset, N. Kinnunen, P. Karvinen, T. K. Hakala and J. J. Saarine, *Mater. Chem. Phys.*, 2022, **277**, 125533.
13 J. Guo, H. van Bui, D. Valdesueiro, S. Yuan, B. Liang and J. R. van Ommen, *Nanomaterials*, 2018, **8**, 61.
14 R. R. Petit, J. Li, B. van de Voorde, S. van Vlierberghe, P. F. Smet and C. Detavernier, *ACS Appl. Mater. Interfaces*, 2021, **13**, 46151–46163.
15 Z. Zhang, A. Simon, C. Abetz, M. Held, A. L. Höhme, E. S. Schneider, T. Segal-Peretz and V. Abetz, *Adv. Mater.*, 2021, **33**, 2105251.
16 E. Edri and H. Frei, *J. Phys. Chem. C*, 2015, **119**, 28326–28334.
17 C. Lin, F. Y. Tsai, M. H. Lee, C. H. Lee, T. C. Tien, L. P. Wang and S. Y. Tsai, *J. Mater. Chem.*, 2009, **19**, 2999–3003.
18 N. Arbell, K. Bauer and Y. Paz, *ACS Appl. Mater. Interfaces*, 2021, **13**, 39781–39790.
19 C. P. Canlas, J. Lu, N. A. Ray, N. A. Grosso-Giordano, S. Lee, J. W. Elam, R. E. Winans, R. P. van Duyne, P. C. Stair and J. M. Notestein, *Nat. Chem.*, 2012, **4**, 1030–1036.
20 R. M. Neubieser, J. L. Wree, J. Jagosz, M. Becher, A. Ostendorf, A. Devi, C. Bock, M. Michel and A. Grabmaier, *Micro Nano Eng.*, 2022, **15**, 100126.
21 M. Z. Ansari, D. K. Nandi, P. Janicek, S. A. Ansari, R. Ramesh, T. Cheon, B. Shong and S. H. Kim, *ACS Appl. Mater. Interfaces*, 2019, **11**, 43608–43621.
22 P. Schmitt, V. Beladiya, N. Felde, P. Paul, F. Otto, T. Fritz, A. Tünnermann and A. V. Szeghalmi, *Coatings*, 2021, **11**, 173.
23 O. Tiurin and Y. Ein-Eli, *Adv. Mater. Interfaces*, 2019, **6**, 1901455.
24 N. E. Richey, C. de Paula and S. F. Bent, *J. Chem. Phys.*, 2020, **152**, 040902.
25 R. L. Puurunen, *J. Appl. Phys.*, 2004, **95**, 4777–4786.
26 P. C. Lemaire, M. King and G. N. Parsons, *J. Chem. Phys.*, 2017, **146**, 052811.
27 R. A. Wind and S. M. George, *J. Phys. Chem. A*, 2010, **114**, 1281–1289.
28 A. Brown, J. Greenwood, C. J. Lockhart de la Rosa, M. C. Rodríguez González, K. Verguts, S. Berms, H. Zhang, B. E. Hirsch, S. De Gendt, A. Delabie, M. Caymax, J. Teyssandier and S. De Feyter, *RSC Nanoscale*, 2021, **13**, 12327–12341.
29 W. Zhang and J. R. Engstrom, *J. Vac. Sci. Technol., A*, 2016, **34**, 01A107.
30 O. V. Bilousov, A. Voznyi, B. Landeke-Wilsmark, M. M. S. Villamayor, T. Nyberg and C. Hägglund, *Chem. Mater.*, 2021, **33**, 2901–2912.
31 J. N. Ding, X. F. Wang, N. Y. Yuan, C. L. Li, Y. Y. Zhu and B. Kan, *Surf. Coat. Technol.*, 2011, **205**, 2846–2851.
32 G. N. Parsons, S. E. Atanasov, E. C. Dandley, C. K. Devine, B. Gong, J. S. Jur, K. Lee, C. J. Oldham, Q. Peng, J. C. Spagnola and P. S. Williams, *Coord. Chem. Rev.*, 2013, **257**, 3323–3331.
33 L. Keskiväli, P. Heikkilä, E. Kenttä, T. Virtanen, H. Rautkoski, A. Pasanen, M. Vähä-nissi and M. Putkonen, *Coatings*, 2021, **11**, 1028.
34 H. An, Y. Du, T. Wang, C. Wang, W. Hao and J. Zhang, *Rare Met.*, 2008, **27**, 243–250.
35 Y. Yang, C. Zhang, C. Lai, G. Zeng, D. Huang, M. Cheng, J. Wang, F. Chen, C. Zhou and W. Xiong, *Adv. Colloid Interface Sci.*, 2018, **254**, 76–93.
36 S. Garg, M. Yadav, A. Chandra, S. Sapra, S. Gahlawat, P. P. Ingole, Z. Pap and K. Hernadi, *RSC Adv.*, 2018, **8**, 29022–29030.

37 M. Náfrádi, K. Hernadi, Z. Kónya and T. Alapi, *Chemosphere*, 2021, **280**, 130636.
38 B. Tryba, M. Toyoda, A. W. Morawski, R. Nonaka and M. Inagaki, *Appl. Catal., B*, 2007, **71**, 163–168.
39 L. Ye, Y. Su, X. Jin, H. Xie and C. Zhang, *Environ. Sci. Nano*, 2014, **1**, 90–112.
40 I. Benisti and Y. Paz, *J. Electrochem. Soc.*, 2019, **166**, H3257.
41 X. Wang, Y. Zhang, C. Zhou, D. Huo, R. Zhang and L. Wang, *Appl. Catal., B*, 2020, **268**, 118390.
42 G. Zhan, J. Li, Y. Hu, S. Zhao, S. Cao, F. Jia and L. Zhang, *Environ. Sci. Nano*, 2020, **7**, 1454–1463.
43 C. Du, S. Nie, W. Feng, J. Zhang, M. Qi, Y. Liang, Y. Wu, J. Feng, S. Dong, H. Liu and J. Sun, *Chemosphere*, 2022, **287**, 132246.
44 Y. Paz and N. Arbell, *US Pat*, 2023/0390751A1, 2023.
45 K. D. Hobart, C. A. Colinge, G. Ayele and F. J. Kub, *Proc. - Electrochem. Soc.*, 2003, **19**, 137.
46 H. Le-The, R. M. Tiggelaar, E. Berenschot, A. van den Berg, N. Tas and J. C. T. Eijkel, *ACS Nano*, 2019, **13**, 6782–6789.
47 H. F. Lü, W. P. Yan, Z. H. Liu and J. C. Li, *Guangpuxue Yu Guangpu Fenxi*, 2016, **36**, 1033–1037.
48 A. Delplanque, E. Henry, J. Lautru, H. Leh, M. Buckle and C. Nogues, *Appl. Surf. Sci.*, 2014, **314**, 280–285.
49 L. Pasternak and Y. Paz, *RSC Adv.*, 2018, **8**, 2161–2172.
50 J. R. Schneider, C. De Paula, N. E. Richey, J. G. Baker, S. T. Oyakhire and S. F. Bent, *Chem. Mater.*, 2022, **34**, 5584–5597.
51 S. Park, S. Y. Kim, Y. Choi, M. Kim, H. Shin, J. Kim and W. Choi, *ACS Appl. Mater. Interfaces*, 2016, **8**, 11189–11193.
52 S. J. McDonnell and R. M. Wallace, *JOM*, 2019, **71**, 224–237.
53 A. Khorsavi, R. Addou, M. Catalano, J. Kim and R. M. Wallace, *Materials*, 2019, **12**, 1056.
54 J. Fan, Y. Shi, H. Liu, S. Wang, L. Luan, L. Duan, Y. Zhang and X. Wei, *Materials*, 2022, **15**, 1794.
55 J. Gong, X. Su, S. Qiu, J. Zhou, Y. Liu, Y. Li, D. Kim, T. Tsai, T. K. Ng, B. S. Ooi and Z. Ma, *J. Appl. Phys.*, 2024, **135**, 115303.
56 Y. Kirihara, T. Yoshida, S. Mikawa, S. Ito, R. Ishikawa and H. Nohira, *ECS Trans.*, 2024, **113**, 35.
57 M. D. Groner, F. H. Fabreguette, J. W. Elam and S. M. George, *Chem. Mater.*, 2004, **16**, 639–645.
58 J. Iqbal, A. Jilani, P. M. Ziaul Hassan, S. Rafique, R. Jafer and A. A. Alghamdi, *J. King Saud Univ., Sci.*, 2016, **28**, 347–354.
59 G. Volp and V. H. Grassian, *Chem. Commun.*, 2013, **49**, 3071–3094.
60 P. V. Brady, *Geochim. Cosmochim. Acta*, 1992, **56**, 2941–2946.
61 F. Shen, L. Zhou, J. Shi, M. Xing and J. Zhang, *RSC Adv.*, 2015, **5**, 4918–4925.
62 Y. Paz, Z. Luo, L. Rabenberg and A. Heller, *J. Mater. Res.*, 1995, **10**, 2842–2848.
63 X. Zhang, Z. Ai, F. Jia and L. Zhang, *J. Phys. Chem. C*, 2008, **112**, 747–753.
64 M. Nussbaum and Y. Paz, *Phys. Chem. Chem. Phys.*, 2012, **14**, 3392–3399.
65 N. Smirnova, T. Fesenko, M. Zhukovsky, J. Goworek and A. Eremenko, *Nanoscale Res. Lett.*, 2015, **10**, 500.
66 Z. S. Seddigi, M. A. Gondal, U. Baig, S. Ahmed, M. Abdulaziz, E. Y. Danish, M. Khaled and A. Lais, *PLoS One*, 2017, **12**, e0172218.
67 S. Imam, R. Adnan, N. H. M. Kaus and M. H. Hussin, *J. Mater. Sci.: Mater. Electron.*, 2019, **30**, 6263–6276.
68 S. Vahabirad and A. Nezamzadeh-Ejhieh, *J. Solid State Chem.*, 2022, **310**, 123018.
69 A. H. Alshehri, K. Mistry, V. H. Nguyen, K. Ibrahim, D. Muñoz-Rojas, M. Yavuz and K. P. Musselman, *Adv. Funct. Mater.*, 2019, **29**, 1805533.